An improved vibration technique for enhancing temperature uniformity and heat transfer in viscous fluid flow

Tian, Shuai; Barigou, Mostafa

DOI:
10.1016/j.ces.2014.11.029

Document Version
Peer reviewed version

Citation for published version (Harvard):
Tian, S & Barigou, M 2015, 'An improved vibration technique for enhancing temperature uniformity and heat transfer in viscous fluid flow', *Chemical Engineering Science*, vol. 123, pp. 609-619. https://doi.org/10.1016/j.ces.2014.11.029

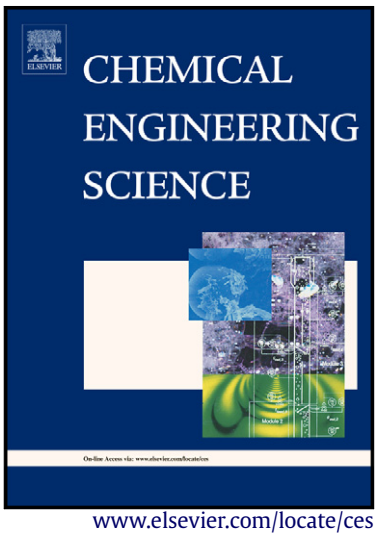

www.elsevier.com/locate/ces

An improved vibration technique for enhancing temperature uniformity and heat transfer in viscous fluid flow

Shuai Tian, Mostafa Barigou

PII: S0009-2509(14)00681-2
DOI: http://dx.doi.org/10.1016/j.ces.2014.11.029
Reference: CES11991

To appear in: *Chemical Engineering Science*

Received date: 11 September 2014
Revised date: 7 November 2014
Accepted date: 12 November 2014

Cite this article as: Shuai Tian, Mostafa Barigou, An improved vibration technique for enhancing temperature uniformity and heat transfer in viscous fluid flow, *Chemical Engineering Science,* http://dx.doi.org/10.1016/j.ces.2014.11.029

AN IMPROVED VIBRATION TECHNIQUE FOR ENHANCING TEMPERATURE UNIFORMITY AND HEAT TRANSFER IN VISCOUS FLUID FLOW

Shuai Tian and Mostafa Barigou*

School of Chemical Engineering, University of Birmingham, Edgbaston, Birmingham, B15 2TT, UK

Abstract

Radial heat transfer in viscous pipe flow is controlled by thermal conduction which leads to a wide radial temperature distribution and slow heating of the core region of the flow. This is highly undesirable in many industrial processes as it results in a grossly uneven distribution of fluid heat treatment. The use of static in-line mixers to promote radial mixing and, thus, heat transfer and temperature uniformity, engenders large pressure drops and the devices are generally prohibited in processes where hygiene is paramount as they are difficult to keep clean. We recently reported a Computational Fluid Dynamics (CFD) study which showed that the superimposing of transverse mechanical oscillations on the steady flow of a viscous fluid in a pipe with an isothermal wall, results in a large enhancement in wall heat transfer, as well as a considerably more uniform radial temperature distribution accompanied by rapid heating of the inner region of the flow. Such a transverse vibration also causes the thermal boundary layer to grow more rapidly and, thus, the temperature profile to develop very rapidly in the axial direction. In this paper, we report on an enhanced vibration technique which combines transverse oscillations with a step rotation of oscillation orientation. The technique produces much more improved effects compared to transverse vibration alone, and it also excels in comparison with the well-known Kenics helical static mixer.

Keywords: CFD; heat transfer enhancement; laminar flow; oscillations; temperature profile; vibration.

* *Corresponding author: Tel: +44 (0)121 414 5277 Fax: +44 (0)121 414 5324 Email: m.barigou@bham.ac.uk*

1. Introduction

When laminar fluid flow in a pipe is accompanied by radial heat transfer, the associated parabolic radial velocity profile leads to a wide radial temperature distribution as heat transfer is controlled by slow conduction. Such conditions pose a considerable challenge in a number of industrial processes, such as the processing of food products, polymer melts and pharmaceutical formulations, where the fluid to be heated (or cooled) is often viscous and temperature dependent. This problem has been recognised for a long time but effective technological solutions are still missing.

In the heating stage of continuous food sterilisation, for example, heat is transferred from the hot pipe wall to the fluid such that the fastest core region of the flow is the coldest, thus, resulting in an undesirable wide variation of product sterility and nutritional quality across the pipe which leads to poor product quality (Jung and Fryer, 1999). The challenge is, therefore, to be able to sterilise the fastest parts in the core region of the pipe without over-processing the slowest parts near the wall so that, ideally, all parts of the fluid should receive equal heat treatment. The optimisation of such thermal processes poses a challenging manufacturing problem. The overriding importance of safety often results in the food being exposed to a more severe process than is desirable from a quality aspect, resulting in poor sensory and nutritional attributes, especially with sensitive products. In the cooling stage of the process the problem is reversed and instead of rapid uniform cooling of the product, the central parts of the flow incur the slowest cooling rates, again leading to significant losses in product quality. These problems become even more complicated when more than one phase is present such as in solid-liquid flows.

To improve the uniformity of the temperature distribution, methods are needed to promote radial mixing in viscous fluid flow. Radial mixing can be enhanced by operating under turbulent flow conditions, but the high fluid viscosities encountered in practice make this proposition impractical and/or uneconomical. Various ways have been proposed to improve heat convection by adding internal screw-thread structures on the wall to disrupt the boundary layer (Shrirao *et al.*, 2013), but such technological solutions are limited by their manufacturing complexity, cost, their high proneness to fouling and clogging, and the difficulty to keep them clean. Similarly, inserts or inline static mixers are used to promote radial fluid mixing and a number of designs exist (Hobbs and Muzzio, 1997; Saatdjian *et al.,* 2012). In viscous flow, such devices can achieve a high degree of fluid mixing but usually at the expense of a high pressure drop. These inserts too are generally prohibited in hygienic processes because of the risk of contamination as their complex geometries also promote fouling and make them difficult to clean.

A number of studies have also demonstrated the effects of pulsating flow on the heat flux and Nusselt number in pipe flows (Gundogdu and Carpinlioglu, 1999). However, the effects on the radial temperature distribution in viscous fluids do not seem to have been reported.

We recently reported a Computational Fluid Dynamics (CFD) study which showed that superimposing transverse mechanical oscillations on the steady flow of a viscous fluid in a pipe with an isothermal wall, results in a large enhancement in wall heat transfer, as well as a considerably more uniform radial temperature distribution accompanied by a substantial heating of the inner region of the flow (Eesa and Barigou, 2010; 2011). Transverse vibration also causes the thermal boundary layer to grow more rapidly and, thus, the temperature profile to develop very rapidly in the axial direction. It should be noted that this type of flow is different from the pulsatile (oscillatory) flow mentioned above.

In this paper, we report on an enhanced vibration technique which combines transverse oscillations with a stepwise angular motion to achieve a high degree of radial fluid mixing, temperature uniformity and heat transfer. We use a validated CFD model to assess and compare the performance of this new method to our previous results using simple transverse vibration, as well as to the performance of the well-known Kenics helical static mixer, one of the best in this category of mixers.

2. CFD model

2.1 . Fluid viscosity

The fluid used is an incompressible, temperature-dependent Newtonian fluid whose viscosity is assumed constant at a given temperature and is described by the well-known Arrhenius relationship:

$$\mu = k_0 exp\left(\frac{E_a}{R_g T}\right) \quad (1)$$

where k_0 is a pre-exponential factor, R_g is the ideal gas constant, T is temperature and E_a is the activation energy for viscosity. The constants k_0 and E_a are determined experimentally and their values for various fluids have been reported in the literature (e.g. Steffe, 1996). These parameters, as well as other physical properties (density ρ, specific heat capacity C_p, and thermal conduct*ivity* λ*)* were assumed constant and their values are given in Table1.

2.2. Transverse oscillations

In our previously reported technique, transverse oscillations are imposed on the pipe wall in a direction perpendicular to the pipe axis, as illustrated in Figure 1(a), and the wall displacement x is described by the function:

$$x = A\sin(\omega t) \tag{2}$$

where A is the amplitude of vibration, t is time, and ω is the angular function of the frequency of vibration, f, such that $\omega=2\pi f$. The linear transversal velocity of the pipe wall is then:

$$u = \frac{dx}{dt} = A\omega\cos(\omega t) \tag{3}$$

In the new enhanced technique being reported here, the pipe is continuously oscillated transversally but the orientation of oscillation is rotated instantly in a stepwise manner by an angle of 45 degrees about the pipe axis, as depicted in Figure 1(b). The time interval, Δt, between change of orientation steps, needs to be optimized for a given set of flow conditions. For the conditions investigated in this work, a value of ~ 10 s was determined via numerical experimentation, thus, the frequency of the step rotation, Ω, is (and is expected to always be) very low compared with the frequency of lateral oscillations; for example, in this case Ω is ~ 0.1 Hz compared to f = 50 Hz.

In all the numerical experiments conducted, under steady state, the flow regime was always laminar with a Reynolds number ($Re = \rho\overline{w}D/\mu$) less than 100, where D is pipe diameter and $\overline{w}$ is mean axial velocity. When the pipe was vibrated, the vibration Reynolds number:

$$Re_v = \frac{\rho A\omega D}{\mu} \tag{4}$$

was always less than 1500, so flow remained laminar throughout, in all the unsteady-state cases studied.

2.3. Governing equations

The governing transport equations can be written in their general form (Bird *et al.*, 1987), thus:

Continuity: $$\nabla \cdot \boldsymbol{U} = 0 \quad (5)$$

Momentum: $$\rho \frac{D\boldsymbol{U}}{Dt} = -\nabla p + \nabla^2 \mu \boldsymbol{U} + \rho \boldsymbol{g} \quad (6)$$

Energy: $$\rho C_p \frac{DT}{Dt} = \lambda \nabla^2 T + \mu \dot{\boldsymbol{\gamma}}^2 \quad (7)$$

where p is fluid pressure, $\boldsymbol{g}$ is gravitational acceleration, $\boldsymbol{U}$ is the velocity field and $\dot{\boldsymbol{\gamma}}$ is the second invariant of the shear rate tensor, defined as $\dot{\boldsymbol{\gamma}} \equiv \left[\frac{1}{2}(\dot{\boldsymbol{\gamma}}:\dot{\boldsymbol{\gamma}})\right]^{\frac{1}{2}}$.

2.4. Mean temperature and pressure

The coefficient of variation is used as a measure of temperature uniformity across the pipe:

$$C_v = \frac{\sigma_T}{\bar{T}} \quad (8)$$

where σ_T is the standard deviation of T. The volume-flowrate weighted mean temperature across the pipe, $\bar{T}$, is obtained by dividing the pipe cross-section into a large number of cells (N = 1860), as shown in Figure 2, which can be identified by their polar coordinates r and θ. The analysis was conducted using this regular grid implemented in MATLAB to avoid the difficulties associated with the complex and varied cell shapes of the computational CFD grid. The temperature and axial velocity in a given cell are denoted by $T(r,\theta)$ and $w(r,\theta)$, respectively, and are considered at their nearly constant time-average values reached after a vibration time equivalent to the fluid residence time in the pipe. Thus, $\sum_{i=1}^{N} w(r,\theta)S(r,\theta) = Q$ represents the volumetric flowrate through a cell, where $S(r,\theta)$ is the cross-sectional area of the cell. The volume-flowrate weighted mean temperature over the pipe cross-section is, therefore, given by:

$$\overline{T} = \frac{1}{Q}\sum_{i=1}^{N} T(r,\theta)w(r,\theta)S(r,\theta) \quad (9)$$

In the limit as $S(r,\theta) \to 0$, i.e. for large N, the uniformity of the temperature distribution over the pipe cross-section can be well described by the standard deviation:

$$\sigma_T = \sqrt{\frac{1}{Q^2}\sum_{i=1}^{N}\left[T(r,\theta)w(r,\theta)S(r,\theta) - \overline{T}w(r,\theta)S(r,\theta)\right]^2} \quad (10)$$

and the coefficient of variation C_v (Eq. 8).

Similarly, to compute the total pressure drop, Δp, along the pipe, the area-weighted mean pressure across the pipe is needed and is computed, thus:

$$\overline{p} = \frac{4}{\pi D^2}\sum_{i=1}^{N} p(r,\theta)S(r,\theta) \quad (11)$$

2.5 Mean wall heat transfer coefficient

The mean wall heat transfer coefficient was calculated using the heat balance equation:

$$\dot{m}C_p(\bar{T}_{out} - T_{in}) = ha\Delta T_m \quad (12)$$

where $\dot{m}$ is the mass flowrate, a is the pipe wall surface area, $\bar{T}_{out}$ is the volume-flowrate averaged temperature at the pipe exit, T_{in} is the uniform temperature at inlet, T_w is the temperature of the isothermal wall, and the log mean temperature difference is defined as $\Delta T_m = \frac{(T_w - \bar{T}_{out}) - (T_w - T_{in})}{\ln[(T_w - \bar{T}_{out})/(T_w - T_{in})]}$ (Sinnott, 2005).

3. CFD simulations

Three-dimensional simulations were set up and executed using the commercial software package ANSYS Workbench 14.5. The flow geometries were created and meshed using the software ICEM, while flow specification, solving and post-processing were all performed using CFX 14.5. The geometry consisted of a straight pipe 30 mm in diameter and 2400 mm in length with three surface boundaries: inlet, outlet, and wall. The geometry was meshed with hexahedral cells. To optimise the mesh size it was necessary to carry out a mesh-independence study; this was done by performing a number of simulations with different mesh sizes, starting from a coarse mesh and refining it until results were no longer dependent on the mesh size. The mesh thus achieved contained approximately 4000 hexahedral cells per centimetre of pipe length and around 1000 cells across the pipe section, giving a mesh size in the core region of about 1 mm. The mesh size near the wall was

progressively reduced down to 0.1 mm to enhance mesh resolution in this region where high velocity and temperature gradients exist. The quality of the mesh measured by its orthogonality and warpage was over 0.75, well above the generally accepted minimum value of 0.4 for a good mesh.

Other simulations were conducted using the same setup with 48 segments of the helical Kenics static mixer, shown in Figure 3, inserted to fill the whole inside of the pipe. The mixer consists of left and right twisting helical elements with a standard length to diameter ratio of 1.5; detailed dimensions are given in Table 2. The same type and size of cell used above in the straight pipe was also used to mesh this geometry, as shown in Figure 4.

In the numerical simulation, a uniform temperature T_{in} = 20 °C and a mass flowrate $\dot{m} = 0.0281\ \mathrm{kg\,s^{-1}}$ were specified at the pipe inlet, and a zero gauge pressure was set at the pipe outlet. The mass flowrate was chosen to give a mean flow velocity $\overline{w} = 4.0\ \mathrm{cm\,s^{-1}}$, which is typical of values used in the processing of viscous food materials (Jung and Fryer, 1999; Steffe, 1996). A constant uniform wall temperature and a no-slip condition were assigned at the wall. In food processing, wall temperatures lower than 180 °C are usually used in practice; here, the bulk of the work was done with T_w = 140 °C, but simulations were also run for T_w = 180 °C to investigate the effects. Other simulation parameters are summarised in Table 3.

The CFD code uses a finite-volume-based method to discretise the governing transport Eqs. (5), (6), (7). In this method, the variable value at an integration point, ϕ_{ip}, is calculated from the variable value at the upwind node, ϕ_{up}, and the variable gradient, $\nabla\phi$, thus

$$\phi_{ip} = \phi_{up} + \beta\nabla\phi\Delta\mathbf{r} \tag{13}$$

where β is a blend factor and $\Delta\boldsymbol{r}$ is the vector from the upwind node to the integration point. With β = 0, the scheme is first order accurate and does not result in non-physical variable values. On the other hand, with β = 1, the scheme is second order accurate but it may result in non-physical values. In the so-called 'High Resolution Advection Scheme' implemented here, the value of β is calculated locally to be as close to 1 as possible without

resulting in non-physical variable values (Barth and Jesperson, 1989). This scheme is therefore intended to satisfy the requirements of both accuracy and boundedness.

Simulations involving steady flow were conducted in the steady-state mode, whereas simulations of vibrational flow were conducted in the transient mode. For a transversely moving boundary, the mesh deformation option in CFX was used which allows the specification of the motion of nodes on boundary regions of the mesh. The motion of all remaining nodes is determined by the so-called displacement diffusion model which is designed to preserve the relative mesh distribution of the initial mesh. The mesh displacement was specified using Eq. (2), and an oscillatory velocity function defined by Eq. (3) was applied at the wall.

The transient scheme used for the solution to march in time was the 'Second Order Backward Euler Scheme'. The simulation was solved over the entire mean residence time of the fluid which is determined by the pipe length and mean flow velocity. For example, for a pipe length of 2400 mm and flow velocity of 4.0 cm s^{-1}, as used here, the fluid residence time in the pipe is 60 s. This time duration was divided into equal time steps, the size of which (1.6667×10^{-3} s) was determined by dividing the vibration cycle into an optimised number of 12 equal time steps. Using a larger number of time steps per vibration cycle did not change the simulation results but prolonged the simulations considerably.

Convergence of the numerical solution was assumed when the root mean square (RMS) of mass, momentum and energy residuals all reached 10^{-4} at each time step which is a good level of accuracy given the complexity of the problem. Achieving this level of convergence typically required 8-12 iterations per time step for vibrational flow and about 50 iterations for steady flow. In practice, however, most of the equations generally reached RMS residual values well below the specified target.

4. Validation of CFD model

Though CFX is a generally well validated code as it is widely used, the computational work reported here was further validated where possible either by comparing results with theoretical solutions or experimental data from the literature. The intention here was to try and validate the CFD model as much as possible so as to maximise confidence in the numerical results. The various stages of the validation process are described below.

4.1 Adiabatic isothermal steady flow through a straight pipe

CFD simulation of the adiabatic isothermal steady flow of inelastic non-Newtonian fluids has been extensively validated in our recent studies for a variety of rheological behaviours, namely power law, Herschel-Bulkley and Bingham plastic, showing excellent agreement with exact analytical solutions within approximately ±1% (Eesa and Barigou, 2008).

4.2 Steady flow through a straight pipe with heat transfer

Three different cases were considered, as follows:

(i) Laminar flow of an isoviscous (i.e. temperature-independent viscosity) Newtonian fluid through the straight pipe described above, was simulated using an isothermal wall at 140°C and a uniform inlet temperature set at 60°C. This is a classic problem which was analytically described and solved by Jakob (1949), as follows:

$$2\overline{w}\left[1-\left(\frac{r}{R}\right)^2\right]\frac{\partial\theta_T}{\partial z}=\frac{\lambda}{\rho C_p}\left(\frac{\partial^2\theta_T}{\partial r^2}+\frac{1}{r}\frac{\partial\theta_T}{\partial r}\right) \tag{14}$$

Subject to boundary conditions:

$\theta_T = 0$ at $r = R$

$\frac{\partial\theta_T}{\partial r} = 0$ at $r = 0$

where r is radial position, R is pipe radius, z is axial position, and the dimensionless temperature θ_T is defined as $\theta_T = (T - T_w)/(T_{in} - T_w)$. We compared the axial temperature variations obtained from the solution of the above differential equation to our CFD predictions at three different radial positions: centre, mid-radius and near the wall. The agreement between CFD and theory was excellent, as shown in Figure 5.

(ii) The numerical solution of Eq. (14) for the case of laminar flow of an isoviscous non-Newtonian power law fluid was first obtained and tabulated by Lyche and Bird (1956) (see also, for example, Chhabra and Richardson (1999) for graphical representation of the data). Comparison of this solution in Figure 6 with the CFD-predicted axial temperature profile for a considerably shear-thinning power law fluid (k = 1 Pa s$^{0.5}$, n = 0.5), shows an excellent agreement.

(iii) Since the variation of viscosity with temperature alters the flow field of the fluid considerably, the velocity profile in the pipe computed by CFD under the conditions of a temperature-dependent viscosity was also validated against experimental results from Kwant *et al*. (1973), as shown in Figure 7. Comparison shows a close agreement between CFD and experiment with a mean difference well within ±3.0%. It should also be noted that in all simulations undertaken in this study, including steady flow and vibrated flow, the energy balance was verified to a very high degree of accuracy (±1.0%).

4.3. Adiabatic isothermal flow in a straight pipe with superimposed vibration

The modelling by CFD of adiabatic isothermal non-Newtonian flow under forced vibration was reported and experimentally validated in our previous studies (Deshpande and Barigou, 2001; Eesa and Barigou, 2008; Eesa, 2009). Comparison with experiment showed that CFD is able to predict such complex flows with a very good accuracy, within approximately ±10%, under a wide range of vibration conditions and for a variety of rheological behaviours, namely power law, Herschel-Bulkley and Bingham plastic. There are, however, no experimental data available on the temperature profile in non-isothermal flows when subjected to vibration. Nonetheless, given the excellent agreement achieved between CFD and theory or experimental results in all the above stages of the validation process, we believe that the present CFD model is sufficiently robust and reliable for the purposes of studying the effects of vibration on the heat transfer characteristics of the flows considered here.

5. Results and discussion

Simulation results for the laminar flow with heat transfer of a Newtonian fluid with temperature-dependent viscosity through a pipe with an isothermal wall are discussed in the following sections for four cases: (i) steady flow through a straight pipe; (ii) steady flow through a straight pipe fitted with a Kenics static mixer; (iii) flow through a straight pipe subjected to transverse oscillations; and (iv) flow through a straight pipe subjected to transverse oscillations with step rotation of vibration orientation.

5.1 Steady flow through a straight pipe

Simulations of the steady pipe flow of a Newtonian fluid with a temperature-dependent viscosity confirmed the usual features of viscous flow, i.e. straight streamlines and a highly non-uniform radial temperature distribution,

as shown in Figure 8. At the pipe exit, there is a substantial cold fluid core which is at temperatures close to the inlet temperature surrounded by outer layers of hot fluid within a sharp temperature gradient. There is little improvement in temperature uniformity along the pipe because of the lack of radial mixing and the reliance on slow thermal conduction for radial heat transfer. The coefficient of radial temperature variation at the pipe exit cross-section defined in Eq. (8) is C_v ~ 0.5.

5.2 Steady flow through a straight pipe fitted with a Kenics static mixer

The Kenics static mixer is widely used in industry to promote radial fluid mixing in pipes, especially where flow is viscous, to improve heat transfer or chemical reactions (Hobbs and Muzzio, 1997; Rahmani et *al*., 2006). This popular static mixer was selected here as a reference for high quality mixing of viscous flow in a pipe. As described in section 3 above, simulations were conducted of the steady flow through the same straight pipe fitted with 48 segments of the Kenics mixer (Figure 3). The flow pattern generated by this configuration is characterised by complex winding fluid streamlines, as shown in Figure 9, and the resulting temperature contour is fairly uniform across the pipe exit section. The static mixer achieves a coefficient of radial temperature variation at the pipe exit of ~ 0.027 which is a vast improvement on steady flow without it (C_v ~ 0.5). The mean fluid temperature increases from 20 °C at the pipe inlet to ~ 61 °C at the exit in the straight pipe without static mixer, but it increases to ~ 108 °C with the static mixer. This substantial improvement in the heating of the fluid was caused by a large enhancement in the mean wall heat transfer coefficient, h, a factor of 3 approximately. However, this enhancement in heat transfer comes at the expense of a large pressure drop, an increase of approximately 8 folds.

5.3 Flow through a straight pipe subjected to transverse oscillations

Simulations of flow in the same straight pipe but with superimposed oscillations in the transverse direction revealed a very different flow pattern. Vibration induces a swirling or spiralling motion in the fluid as clearly represented by the complex fluid trajectories depicted in Figure 10(b). Such a flow pattern is characterised by significant vortical structures which cause considerable radial mixing, thus, leading to a much more uniform temperature distribution, as shown in Figure 10(a). Thus, the coefficient of radial temperature variation, improved from C_v ~ 0.5 for simple steady flow to ~ 0.07 for vibrated flow. The mean fluid temperature increased from 20 °C at the inlet of the straight pipe to ~ 61 °C at the exit when flow was steady, but it increased to ~ 117 °C when flow was vibrated. This considerable improvement in the heating of the fluid was caused by

a large enhancement in the mean wall heat transfer coefficient, a factor of 4 approximately. In recent work (Eesa and Barigou, 2010; 2011) we showed that these effects depend, amongst other factors, on the vibration amplitude and frequency but are more sensitive to the amplitude than the frequency. In fact, results showed that the scale of vorticity nearly doubled as *A/D* increased from 0.05 to 0.1. Since the strength of transverse fluid motion is directly responsible for the observed radial mixing, this explains its strong dependence on *A/D*.

Whilst the imposition of transverse oscillations gives a substantial improvement in heat transfer compared with simple steady flow, and despite the considerable improvement in radial mixing, the degree of mixing averaged across the pipe section (C_v ~ 0.07) is still short of the level achieved by the static mixer (C_v ~ 0.027), albeit the pressure drop caused by the latter system is a factor of ~ 5.6 higher.

The vibrated flow is characterized by four salient symmetrical regions of relatively colder fluid being trapped in swirling flow inside clearly delineated vortices located in the four quadrants of the pipe cross-section, as shown in Figure 10, which hamper fluid mixing. The local temperature in the centre of these vortex regions is ~ 99 °C compared to ~ 128 °C in the centre of the pipe. Whilst the results reported in our previous study on heat transfer enhancement via vibration are in agreement with present findings, it should be noted that these relatively cold vortex regions were not clearly apparent in our previous analysis (Eesa and Barigou, 2010; 2011). However, it has been possible to identify them here because of the superior quality of the hexahedral mesh used in the present simulations compared with the tetrahedral mesh used previously. Hexahedral meshes are known to achieve a higher solution accuracy than tetrahedral meshes for the same cell amount, and provide the best resolution of the boundary layer close to walls with significantly fewer cells. Hexahedral elements also reduce numerical diffusion, aid convergence, and have important computing cost and stability advantages over tetrahedral elements (see for example, Biswas and Strawn, 1998; Tadepalli *et al*., 2011).

The velocity field in a plane normal to the direction of flow is depicted in Figure 11. The velocity vector plot shows how hot fluid is forced by the transverse oscillations to flow inwards from the wall and recirculate around the vortex regions before returning to the wall. Therefore, better fluid mixing is needed in these regions for optimal heat transfer and temperature uniformity. To improve on this situation, we propose to rotate the orientation of transverse oscillation in a stepwise manner by an angle of 45-degrees, as described in section 2.2 and illustrated in Figure 1(b), in order to force the centres of the four cold regions to move around and, hence,

enable the relatively cold fluid in these regions to better mix with hotter fluid flowing inwards from the wall.

5.4 Flow through a straight pipe subjected to transverse oscillations with a superimposed step rotation of vibration orientation

This regime of flow creates much more intense radial fluid mixing, as demonstrated by the fluid trajectories shown in Figure 12(b). As a result, the cold vortex regions have disappeared from the temperature contour plot and a much improved temperature distribution is obtained, as depicted in Figure 12(a). A comparison is drawn in Table 4 between the four regimes of flow studied, i.e. simple steady pipe flow, steady flow with a Kenics static mixer, vibrated flow, and vibrated flow with a superimposed step rotation of orientation. The vibrated flow with a step rotation of oscillation orientation exhibits huge improvements in heat transfer characteristics compared with simple steady flow in a straight pipe. For example, the uniformity of the temperature distribution is vastly improved and the heat transfer coefficient h is enhanced by ~ 5 folds. With respect to vibration alone, the step rotation of oscillation orientation brings about considerable improvements in these parameters; for example, C_v reduces from ~ 0.07 down to ~ 0.02. Even when compared with flow through the Kenics mixer, C_v shows a significant improvement from ~ 0.027 to ~ 0.02, whilst the pressure drop incurred in the pipe fitted with the static mixer is much greater, ~ 6.2 times. It is worth noting that when using static mixers, C_v ~ 0.05 is generally accepted in the literature as a target level for good fluid mixing (Reed *et al.*, 2002). This corroborates the conclusion that transverse vibration with step changes in orientation provides an elegant non-invasive technique for enhancing radial fluid mixing and heat transfer.

The effects of vibration on the development of the thermal boundary layer are depicted in Figure 13 where the mean temperature profile along the pipe is shown to develop fastest in the vibrated flow with step rotation of orientation. Such information is also graphically illustrated in the form of mean temperature variations as a function of axial position in Figure 14, where vibration with rotation surpasses the other flow regimes by a wide margin.

To put the above results in context, in order to obtain the same mean temperature achieved by transverse vibration with step rotation of orientation at the exit of the 2.4 m pipe used here, the length of pipe would have to be, approximately, 26 m in simple steady flow, 18 m compared with transverse vibration alone, and 14 m with the Kenics static mixer. However, to achieve the same level of temperature uniformity at exit, i.e. the same C_v, approximately 40 m would be needed in simple steady, 22 m with transverse vibration

alone, and 35 m with the Kenics mixer.

The effect of varying the frequency, Ω, of the step rotation of oscillation orientation was investigated and radial temperature profile results are displayed in Figure 15. It turns out that the value of this frequency is quite significant in achieving the highest mean temperature at the pipe exit, the best temperature uniformity across radius, and the best wall heat transfer coefficient whilst Δp is more or less unchanged (Table 5). As discussed above, efficient radial fluid mixing is achieved through transverse vibration by forcing the hot liquid to continuously flow from the wall to the centre of the pipe, mix with fluid in the cold regions, before returning to the wall. Out of the frequency values which were tested for the flow conditions investigated, the best temperature uniformity (and correspondingly the best temperature development along the pipe) corresponded to $\Omega = 0.1$ Hz (i.e. a time interval between rotation steps of $\Delta t = 10$ s). The value of this optimum step rotation frequency is expected to depend on process conditions, however.

As shown in Figure 16, with higher frequencies (e.g. $\Omega = 0.2$ Hz; $\Delta t = 5$ s; distance travelled $z = 0.2$ m) the hot fluid does not get to reach the pipe centre, thus, there is insufficient mixing of the hot fluid flowing inwards from the wall with cold fluid conveyed in the cold vortex regions before recirculating back; whilst with lower frequencies (e.g. $\Omega = 0.067$ Hz; $\Delta t = 15$ s; distance travelled $z = 0.6$ m) the cold vortex regions are moved around too slowly for optimum heat transfer to take place from the hot fluid flowing inwards from the wall; thus, the temperature gradient between cold and hot fluid is not as high as it could be for efficient heat transfer. In this case, a rotation frequency of 0.1 Hz (i.e. $\Delta t = 10$ s; distance travelled $z = 0.4$ m) gives the best condition for radial mixing and heat transfer.

Simulations for a higher wall temperature of 180 °C gave similar results under all conditions of flow investigated, respectively; however, because of the large temperature gradient across the pipe radius, to achieve a degree of temperature uniformity similar to that attained in the 140 °C case required a slightly longer pipe (~ 2.6 m).

5.5. Mechanical energy consumption through vibration

The mechanism of superimposing a step rotation of oscillation orientation on the vibrated flow should not be difficult to implement in practice and should provide an elegant technological solution for enhancing heat

transfer operations in viscous flows, as discussed above. The technique excels in comparison with the Kenics helical mixer which suffers from its unsuitability for hygienic processes, as well as the relatively high energy losses caused by the large pressure drops it engenders.

To complete the evaluation of the vibration process, we estimate the mechanical energy involved in implementing the mechanical oscillations, as shown in Appendix A. The estimation for the flow case discussed above indicates that the power required to run the vibration process is rather modest (~ 130 W), and the benefits in terms of temperature uniformity and enhanced heat transfer should far outweigh this additional cost.

6. Conclusions

Forced transverse vibration superimposed on the steady laminar flow of a fluid in a pipe with an isothermal wall generates a vigorous swirling fluid motion represented by a strong vorticity field and complex spiralling fluid streamlines and trajectories. The method has been shown to have substantial benefits for heat transfer including a large (several folds) increase in wall heat transfer, a much more uniform radial temperature profile, a rapid development of the temperature profile along the pipe, rapid heating of the core region of the flow, and relatively short processing pipes.

A new enhanced technique has been introduced in this work which combines transverse vibration with a step rotation of oscillation orientation. This technique produces much more improved effects compared to transverse vibration alone, resulting in much shorter processing pipes. It also excels in comparison with the well-known Kenics helical static mixer which has the disadvantages of being unsuitable for hygienic fluid processing and causes large pressure drops. On the other hand, the mechanical power input associated with the vibration process is modest.

Appendix A – Mechanical energy consumption through vibration

From equation (2) which describes the pipe wall displacement, the acceleration can be obtained as:

$$\dot{u} = \frac{\mathrm{d}u}{\mathrm{d}t} = \frac{\mathrm{d}^2x}{\mathrm{d}t^2} = -A\omega^2\sin(\omega t) \tag{A1}$$

The vibration force is given by Newton's second law of motion, thus:

$$F = m \times \dot{u} = -m \times A\omega^2\sin(\omega t) \tag{A2}$$

where m is the mass of the pipe full of fluid. The elemental work developed across the infinitesimal displacement $\mathrm{d}x$ is given by:

$$\mathrm{d}W = F \times \mathrm{d}x$$

$$\mathrm{d}W = -m \times A\omega^2\sin(\omega t) \times A\omega\cos(\omega t) \times \mathrm{d}t \tag{A3}$$

So through a whole oscillation cycle, ignoring any energy losses due to friction or imperfect transmission, the total work is obtained from:

$$W = \int_0^{\frac{1}{f}} -mA^2\omega^3\sin(\omega t)\cos(\omega t)\,\mathrm{d}t \tag{A4}$$

$$W = \int_0^{\frac{1}{4f}} -mA^2\omega^3\sin(\omega t)\cos(\omega t)\,\mathrm{d}t + \int_{\frac{1}{4f}}^{\frac{1}{2f}} -mA^2\omega^3\sin(\omega t)\cos(\omega t)\,\mathrm{d}t + \int_{\frac{1}{2f}}^{\frac{3}{4f}} -mA^2\omega^3\sin(\omega t)\cos(\omega t)\,\mathrm{d}t + \int_{\frac{3}{4f}}^{\frac{1}{f}} -mA^2\omega^3\sin(\omega t)\cos(\omega t)\,\mathrm{d}t$$

The total algebraic work given by the above expression through a complete vibration cycle amounts to zero as the 2nd integral negates the 1st integral, and the 4th integral negates the 3rd integral. Note that the 2nd and 4th integrals represent work dissipated during the deceleration parts of the cycle. Therefore, the net work input in one cycle is given by the sum of the 1st and 3rd integrals, thus:

$$W = -mA^2\omega^2 \quad \text{(A5)}$$

Assuming, for example, a pipe wall thickness of 2.5 mm, a stainless steel density of 8000 kg m^{-3}, and using the values of the various other parameters introduced for the flow case set out above, the power consumption turns out to be rather modest:

$$\boldsymbol{\mathcal{P}} = f \times mA^2\omega^2 \approx 130 \text{ W} \quad \text{(A6)}$$

Acknowledgements

Shuai Tian's PhD research was funded by a China Government & University of Birmingham scholarship.

Nomenclature

A	Vibration amplitude, m
C_p	Specific heat capacity, J kg^{-1} K^{-1}
E_a	Activation energy for viscosity, J mol^{-1}
f	Vibration frequency, Hz
h	mean wall heat transfer coefficient, W m^{-2} K^{-1}
k_0	Pre-exponential factor, Pa s
p	Pressure, Pa
Δp	Pressure drop, Pa
r	Radial position, m
R	Radius of pipe, m
R_g	Gas constant, J mol^{-1} K^{-1}
t	Time, s
Δt	Time interval, s
T	Temperature, °C
$\bar{T}$	Volume-flowrate weighted mean temperature, °C
T_{in}	Inlet temperature, °C
$\bar{T}_{out}$	Volume-flowrate averaged temperature at the pipe exit, °C
T_w	Wall temperature, °C
u	Velocity in radial direction, m s^{-1}
w	Velocity in axial direction, m s^{-1}
$\overline{w}$	Mean axial velocity at inlet, m s^{-1}
x	Wall displacement, m
z	Axial position, m

Greek symbols

μ Temperature-dependent viscosity of Newtonian fluid, Pa s
ρ Density, kg m^{-3}
λ Thermal conductivity, W m^{-1} K^{-1}
θ_T Dimensionless temperature, -
θ Azimuthal position, rad or deg
ω Angular function of frequency of vibration, rad s^{-1}
Ω Frequency of step rotation of vibration orientation, Hz

8. References

Barth, T. J., Jesperson D. C. (1989). The design and application of upwind schemes on unstructured meshes. AIAA. 1-12.

Bird, R. B., Armstrong, R. C., Hassager, O. & Curtiss, C.F. 1987. *Dynamics of polymeric liquids*, Vol. 1: Fluid Mechanics. 2nd Edition, John Wiley.

Biswas, R., & Strawn, R. C. (1998). Tetrahedral and hexahedral mesh adaptation for CFD problems. Applied Numerical Mathematics, 26(1–2), 135-151.

Chhabra, R. P. & Richardson, J. F. 1999. *Non-Newtonian flow in the process industries: Fundamentals and engineering applications*. Butterworth Heinemann.

Deshpande, N. S., & Barigou, M. (2001). Vibrational flow of non-Newtonian fluids. Chemical Engineering Science, 56(12), 3845-3853.

Eesa, M., & Barigou, M. (2008). CFD analysis of viscous non-Newtonian flow under the influence of a superimposed rotational vibration. Computers & Fluids, 37(1), 24-34.

Eesa, M. (2009). CFD studies of complex fluid flows in pipes. Ph.D. thesis. University of Birmingham.

Eesa, M., & Barigou, M. (2010). Enhancing radial temperature uniformity and boundary layer development in viscous Newtonian and non-Newtonian flow by transverse oscillations: A CFD study. Chemical Engineering Science, 65(6), 2199-2212.

Eesa, M., & Barigou, M. (2011). CFD simulation of transverse vibration effects on radial temperature profile and thermal entrance length in laminar flow. AIChE Journal, 57(1), 51-56.

Gundogdu, M. Y., & Carpinlioglu, M. O. (1999). Present state of art on pulsatile flow theory - (Part 1: Laminar and transitional flow regimes). JSME International Journal Series B-Fluids and Thermal Engineering, 42(3), 384-397.

Hobbs, D. M., & Muzzio, F. J. (1997). The Kenics static mixer: a three-dimensional chaotic flow. Chemical Engineering Journal, 67(3), 153-166.

Jakob, M. (1949). *Heat transfer.* Wiley.

Jung, A., & Fryer, P. J. (1999). Optimising the quality of safe food: Computational modelling of a continuous sterilisation process. Chemical Engineering Science, 54(6), 717-730.

Kwant, P. B., Fierens, R. H. E., & Vanderle. A. (1973). Non-isothermal laminar pipe flow - II. Experimental. Chemical Engineering Science, 28(6), 1317-1330.

Lyche, B. C., & Bird, R. B. (1956). The Graetz-Nusselt problem for a power-law non-Newtonian fluid. Chemical Engineering Science, 6(1), 35-41.

Rahmani, R. K., Keith, T. G., & Ayasoufi, A. (2006). Numerical study of the heat transfer rate in a helical static mixer. Journal of Heat Transfer, 128(8), 769.

Reed, G. F., Lynn, F., & Meade, B. D. (2002). Use of coefficient of variation in assessing variability of quantitative assays. Clinical and Diagnostic Laboratory Immunology, 9(6), 1235-1239.

Saatdjian, E., Rodrigo, A. J. S., & Mota, J. P. B. (2012). On Chaotic Advection in a Static Mixer. Chemical Engineering Journal, 187(0), 289- 298.

Shrirao, P. N., Sambhe, R. U., & Bodade, P. R. (2013). Convective Heat Transfer Analysis in a Circular Tube with Different Types of Internal Threads of Constant Pitch. International Journal of Engineering and Advanced Technology, 2(3), 335-340.

Sinnott, R. K. (2005). *Chemical Engineering Design: Chemical Engineering*. Elsevier Science.

Steffe, J. F. (1996). *Rheological methods in food process engineering*. 2nd Edition. Freeman Press.

Tadepalli, S. C., Erdemir, A., & Cavanagh, P. R. (2011). Comparison of hexahedral and tetrahedral elements in finite element analysis of the foot and footwear. Journal of Biomechanics, 44(12), 2337-2343.

Table 1: Rheological parameters used.

k_0 (Pa s)	E_a (J mol^{-1})	R_g (J mol^{-1} K^{-1})	ρ (kg m^{-3})	C_p (J kg^{-1} K^{-1})	λ (W m^{-1} K^{-1})	μ (Pa s)	
						20°C	140°C
5.0×10^{-7}	35000	8.314	998	4180	0.668	0.868	0.0134

Table 2: Dimensions of Kenics static mixer (Figure 3).

Segment length (mm)	Gap width (mm)	Element length (mm)	Mixer diameter (mm)	Element thickness (mm)	Twist angle (rad)
50	2.5	45	30	1	π

Table 3: Simulation parameters used.

Flow regime	Simulation time t (s)	Vibration frequency f (Hz)	Vibration amplitude A (mm)	Frequency of step rotation of vibration orientation Ω (Hz)	Temperature of isothermal wall T_w (°C)
Steady flow through straight pipe	-	-	-	-	140, 180
Steady flow through Kenics static mixer	-	-	-	-	140, 180
Transverse oscillations	60	50	2	-	140, 180
Transverse oscillations with step rotation of vibration orientation	60	50	2	0.2, 0.1, 0.067	140, 180

Table 4: Comparison of the four different flow regimes studied (T_w =140 °C).

	Steady flow through straight pipe	**Steady flow through Kenics static mixer**	**Flow with transverse oscillations**	**Flow with transverse oscillations and step rotation of vibration orientation**
Mean temperature at exit $\overline{T}_{out}$ (°C)	61.3	108.1	116.8	126.5
Coefficient of radial temperature variation C_v (-)	0.49	0.026	0.069	0.021
Mean wall heat transfer coefficient h (W m^{-2} K^{-1})	297.8	935.3	1160.7	1544.7
Pressure drop Δp (Pa)	195.0	1500.7	267.5	244.0

Table 5: Effects of frequency of step rotation of vibration orientation.

Step rotation frequency Ω (Hz)	**0.2**	**0.1**	**0.067**
Mean temperature at pipe exit $\overline{T}_{out}$ (°C)	121.1	126.5	121.3
Coefficient of radial temperature variation at pipe exit C_v (-)	0.045	0.021	0.062
Mean wall heat transfer coefficient h (W m^{-2} K^{-1})	1304.0	1544.8	1311.1
Pressure drop Δp (Pa)	241.2	244.0	228.5

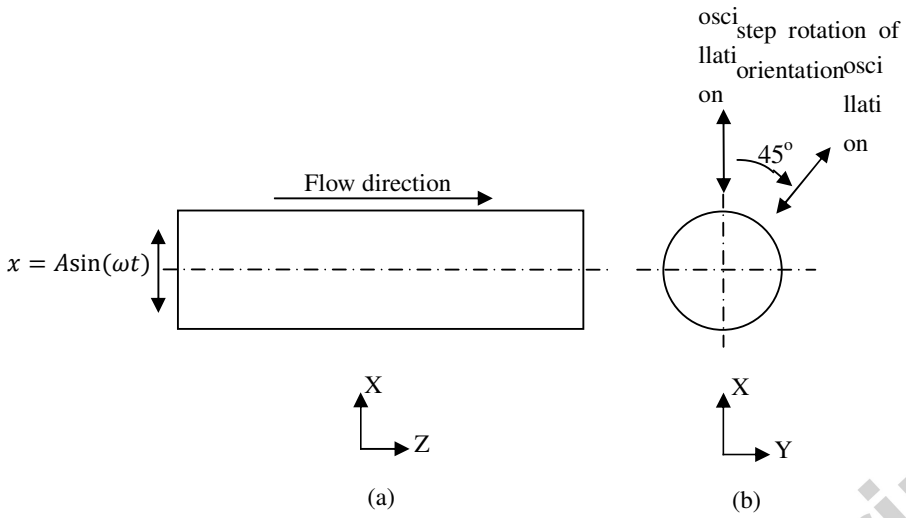

Figure 1: Viscous flow in a straight pipe: (a) under transverse vibration; (b) under transverse vibration coupled with superimposed 45-degree step rotation of vibration orientation.

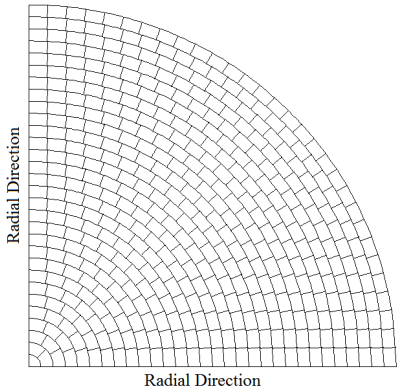

Figure 2: Illustration of grid used for evaluation of volume-flowrate weighted mean temperature and area-weighted pressure over pipe section (total number of cells, $N = 1860$ cells).

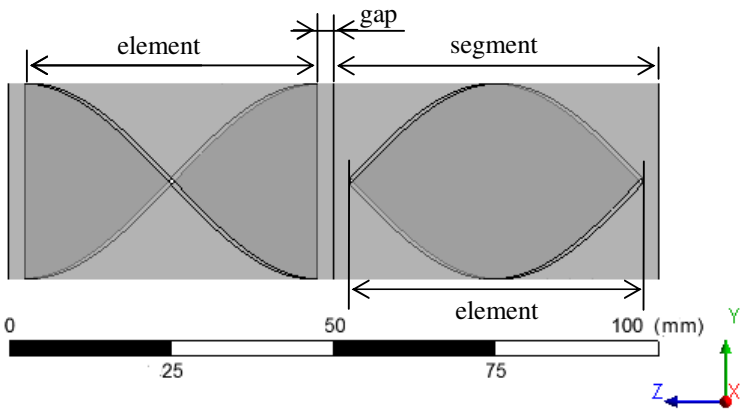

Figure 3: Geometry of helical Kenics static mixer showing two adjacent mixer segments.

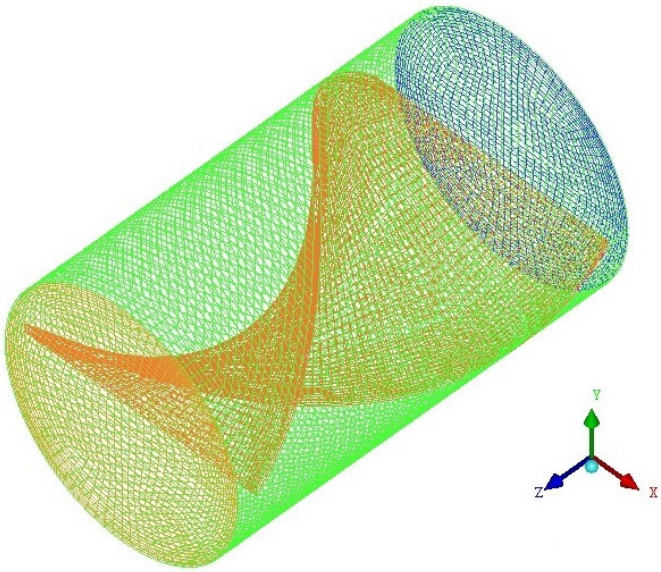

Figure 4: Schematic mesh of pipe fitted with Kenics static mixer.

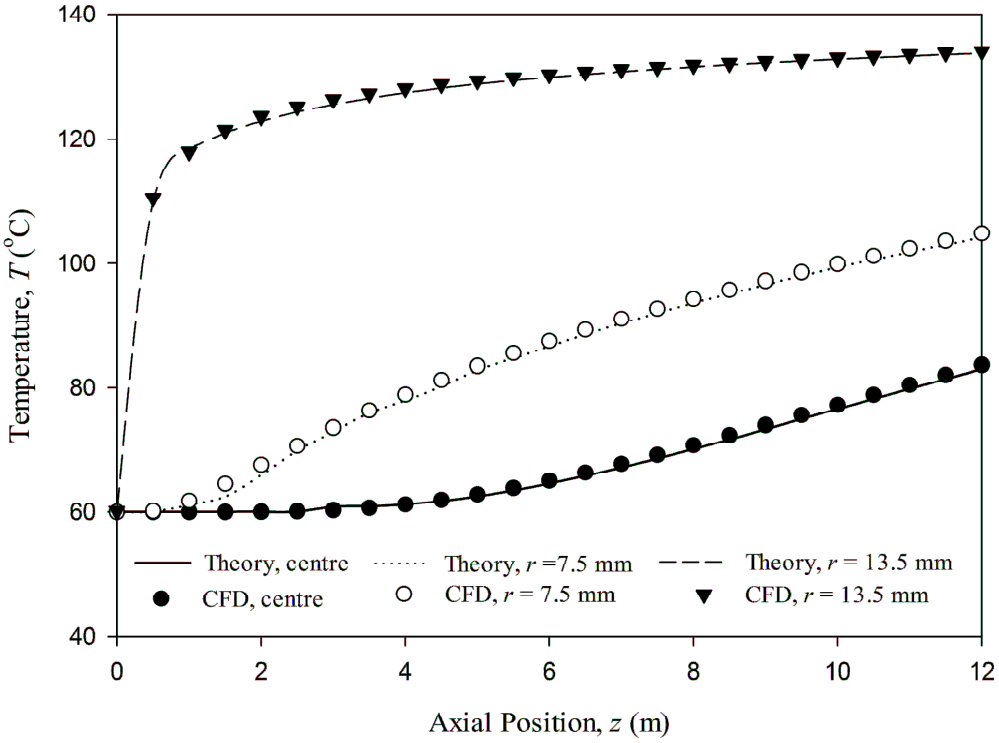

Figure 5: Comparison of CFD-predicted and theoretical (Eq. 14) axial temperature profiles at three different radial positions for isoviscous Newtonian fluid in steady laminar pipe flow: T_{in} = 60 °C; T_w = 140 °C; D = 30 mm; $\bar{w}$ = 4.0 cm s^{-1}; μ = 0.001 Pa s; ρ = 998 kg m^{-3}; C_p = 4180 J kg^{-1} K^{-1}; λ = 0.6 W m^{-1} K^{-1}.

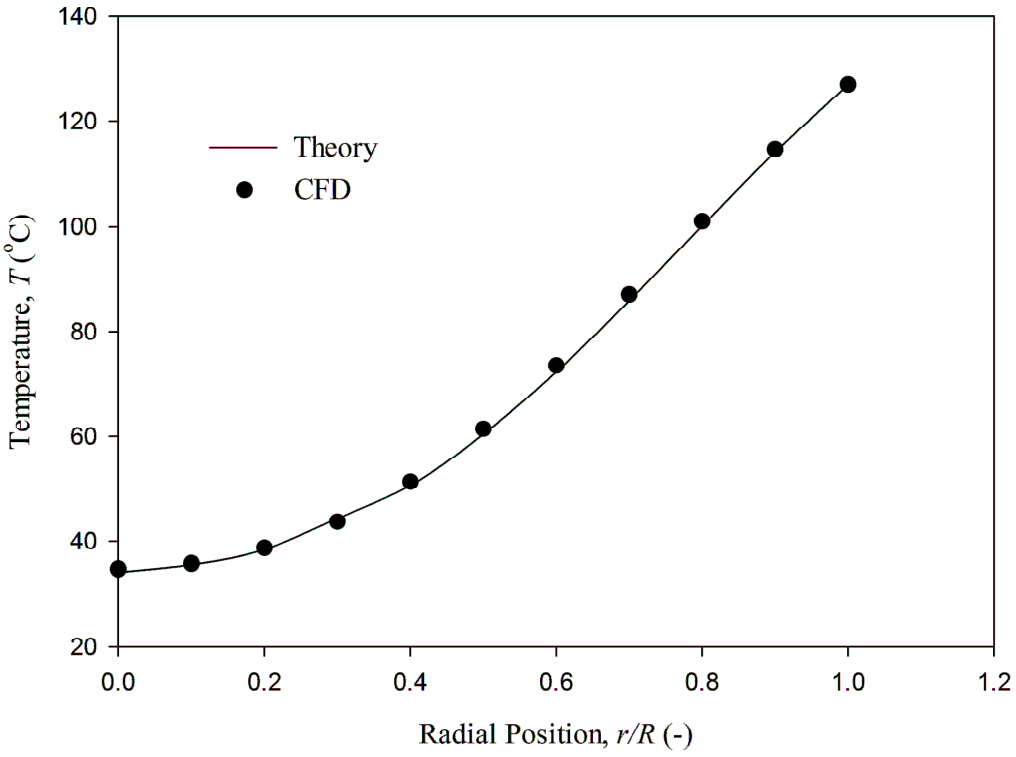

Figure 6: Comparison of CFD-predicted and theoretical (Eq. 14) axial temperature profiles for isoviscous non-Newtonian power law fluid in steady laminar pipe flow: T_{in} = 27 °C; T_w = 127 °C; D = 30 mm; $\overline{w}$ = 1.0 cm s^{-1}; ρ = 998 kg m^{-3}; k = 1 Pa s$^{0.5}$; n = 0.5; C_p = 4180 J kg^{-1} K^{-1}; λ = 0.6 W m^{-1} K^{-1}.

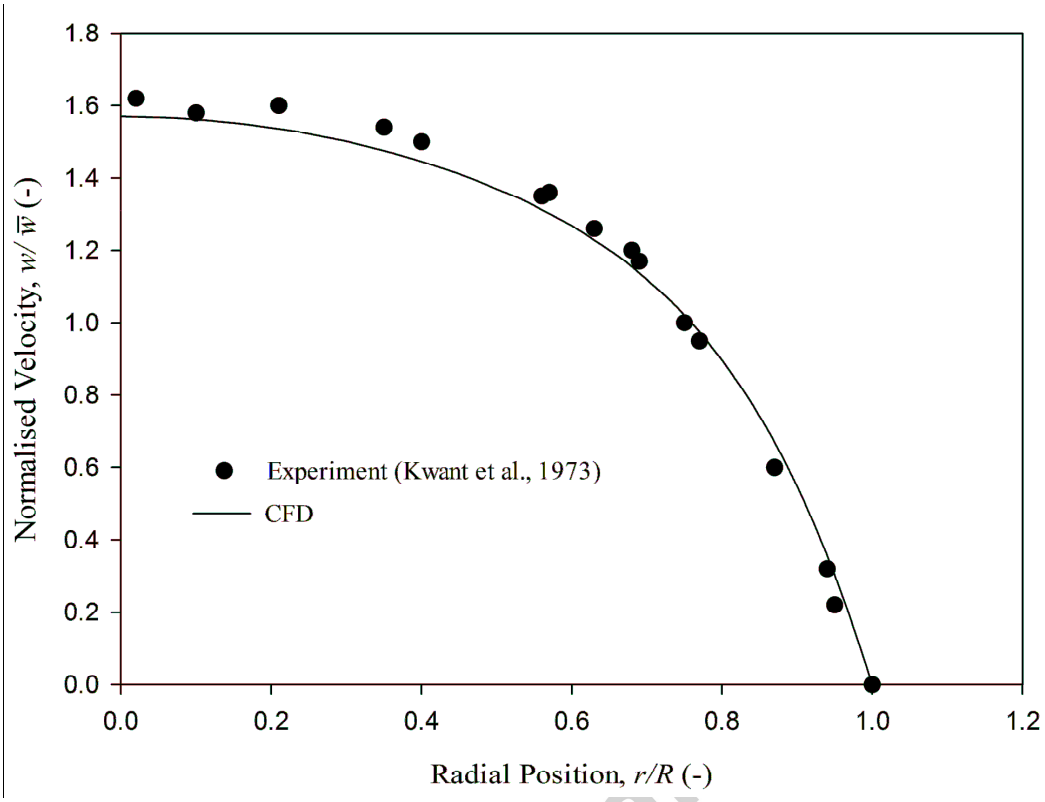

Figure 7: Comparison of CFD-predicted and experimental velocity profiles for a temperature-dependent Newtonian fluid in steady pipe flow with heat transfer: T_{in} = 27 °C; T_w = 127 °C; D = 30 mm; $\overline{w}$ = 2.0 cm s^{-1}; μ = 1.3exp[(T – 25 °C)/(T_w - T_{in})] Pa s; ρ = 998 kg m^{-3}; C_p = 4180 J kg^{-1} K^{-1}; λ = 0.6 W m^{-1} K^{-1}.

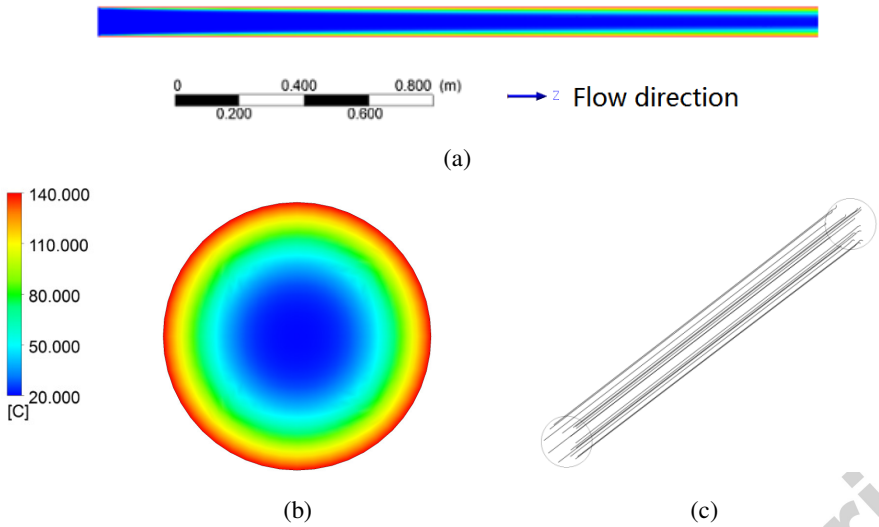

Figure 8: Steady viscous flow of a temperature-dependent Newtonian fluid in a straight pipe: (a) temperature distribution along the pipe; (b) temperature distribution at pipe exit; (c) fluid streamlines.
T_{in} = 20 °C; T_w = 140 °C; D = 30 mm; L = 2400 mm; = 4.0 cm s^{-1}; $\mu = k_0 \exp(E_a/R_g T)$ Pa s; ρ = 998 kg m^{-3}; C_p = 4180 J kg^{-1} K^{-1}; λ = 0.668 W m^{-1} K^{-1}.

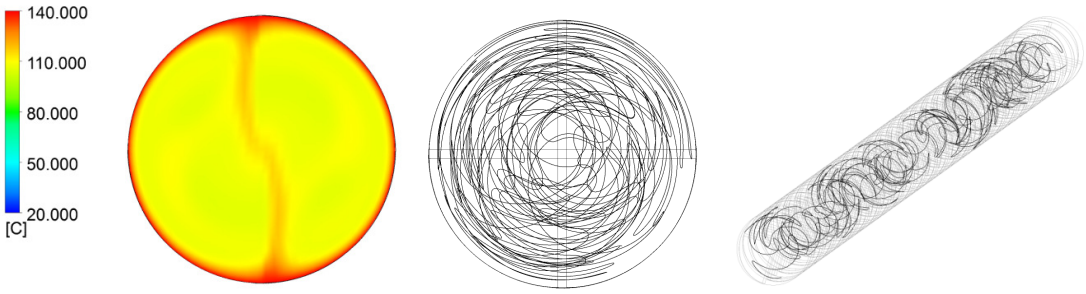

(a) (b)

Figure 9: Viscous flow of a temperature-dependent Newtonian fluid in a straight pipe fitted with a Kenics static mixer: (a) temperature distribution at pipe exit; (b) fluid trajectories.
T_{in} = 20 °C; T_w = 140 °C; D = 30 mm; L = 2400 mm; = 4.0 cm s^{-1}; $\mu = k_0 \exp(E_a/R_g T)$ Pa s; ρ = 998 kg m^{-3}; C_p = 4180 J kg^{-1} K^{-1}; λ = 0.668 W m^{-1} K^{-1}.

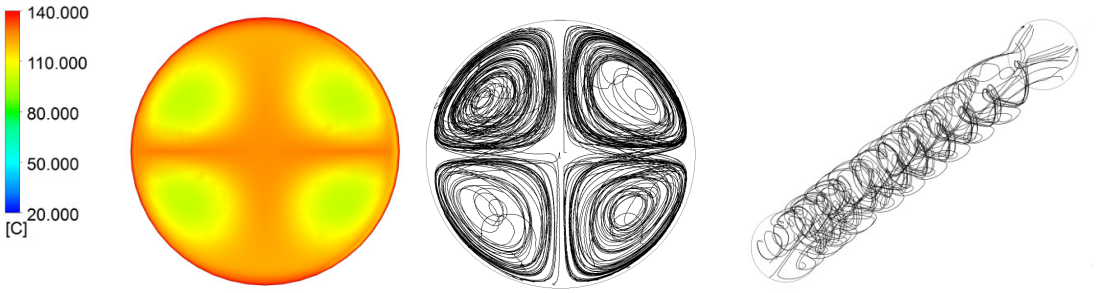

(a) (b)

Figure 10: Viscous flow of a temperature-dependent Newtonian fluid in a straight pipe subjected to transverse oscillations: (b) temperature distribution at pipe exit; (b) fluid trajectories.
T_{in} = 20 °C; T_w = 140 °C; D = 30 mm; L = 2400 mm; = 4.0 cm s^{-1}; $\mu = k_0 \exp(E_a/R_g T)$ Pa s; ρ = 998 kg m^{-3}; C_p = 4180 J kg^{-1} K^{-1}; λ = 0.668 W m^{-1} K^{-1}; A = 2 mm; f = 50 Hz.

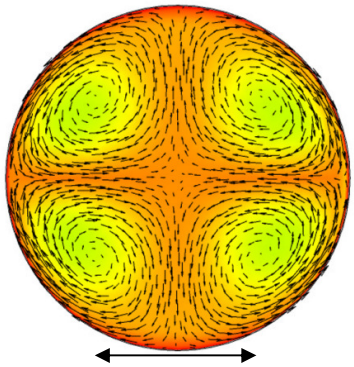

Figure 11: Velocity vector plot superimposed on temperature distribution across the oscillated pipe.

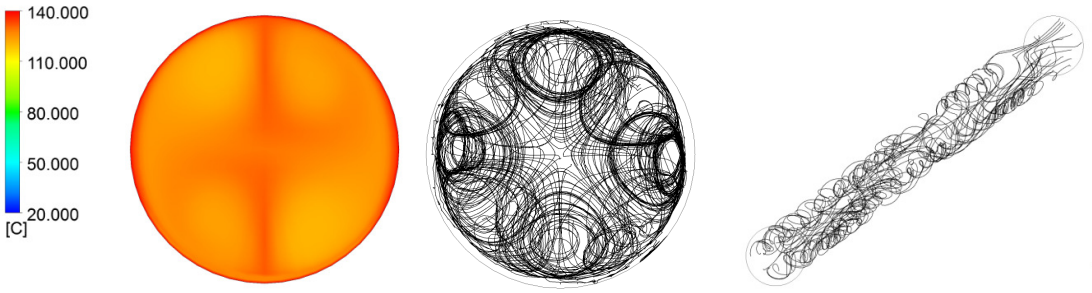

(a) (b)

Figure 12: Viscous flow of a temperature-dependent Newtonian fluid in a straight pipe subjected to transverse oscillations with a superimposed step rotation of vibration orientation: (a) temperature distribution at pipe exit; (b) fluid trajectories.

T_{in} = 20 °C; T_w = 140 °C; D = 30 mm; L = 2400 mm; = 4.0 cm s^{-1}; $\mu = k_0 \exp(E_a/R_g T)$ Pa s; ρ = 998 kg m^{-3}; C_p = 4180 J kg^{-1} K^{-1}; λ = 0.668 W m^{-1} K^{-1}; A = 2 mm; f = 50 Hz.

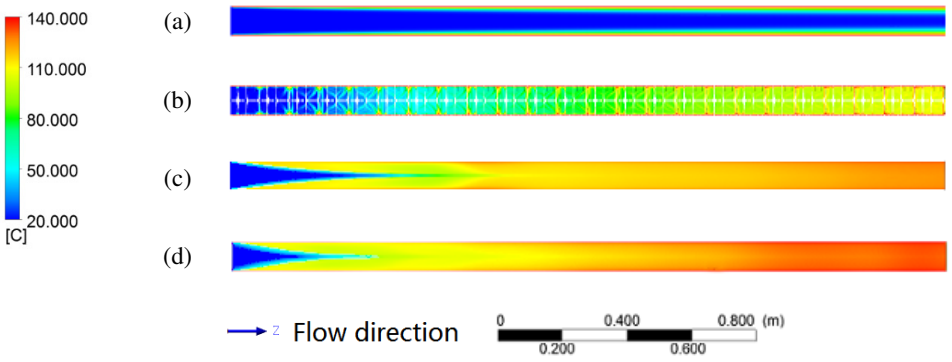

Figure 13: Development of azimuthally-averaged temperature profile along the pipe: (a) simple steady flow; (b) steady flow through helical static mixer; (c) flow with transverse oscillations; (d) flow with transverse oscillations and step rotation of vibration orientation.

T_{in} = 20 °C; T_w = 140 °C; D = 30 mm; L = 2400 mm; = 4.0 cm s^{-1}; $\mu = k_0 \exp(E_a/R_g T)$ Pa s; ρ = 998 kg m^{-3}; C_p = 4180 J kg^{-1} K^{-1}; λ = 0.668 W m^{-1} K^{-1}; A = 2 mm; f = 50 Hz.

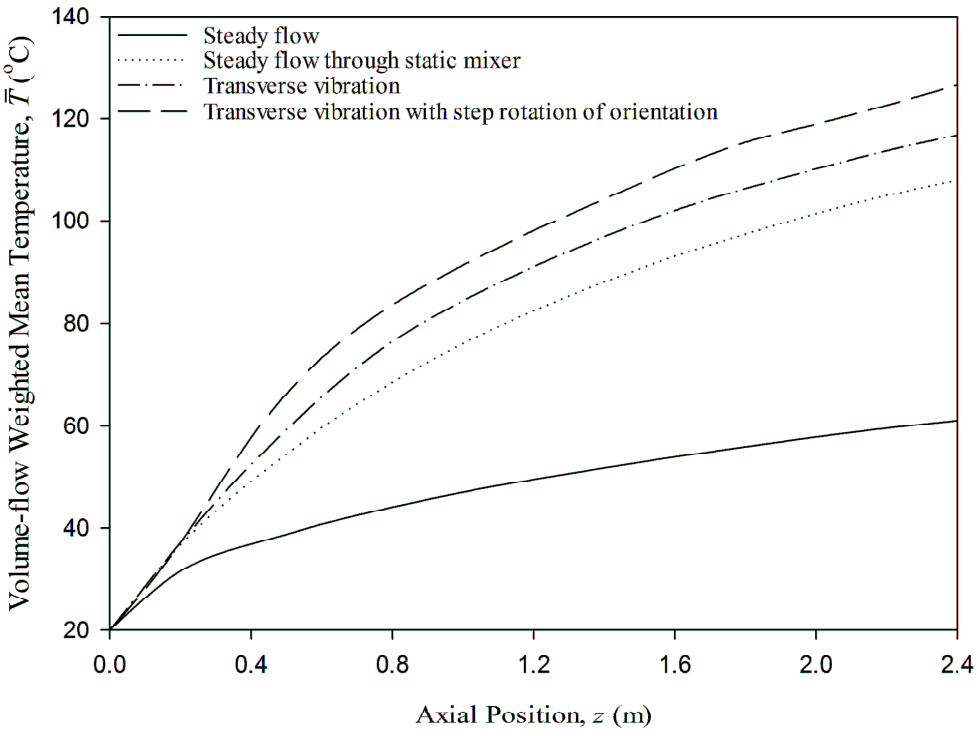

Figure 14: Mean temperature development along the pipe: T_{in} = 20 °C; T_w = 140 °C; D = 30 mm; L = 2400 mm; $\bar{w}$ = 4.0 cm s^{-1}; $\mu = k_0 \exp(E_a/R_g T)$ Pa s; ρ = 998 kg m^{-3}; C_p = 4180 J kg^{-1} K^{-1}; λ = 0.668 W m^{-1} K^{-1}; A = 2 mm; f = 50 Hz.

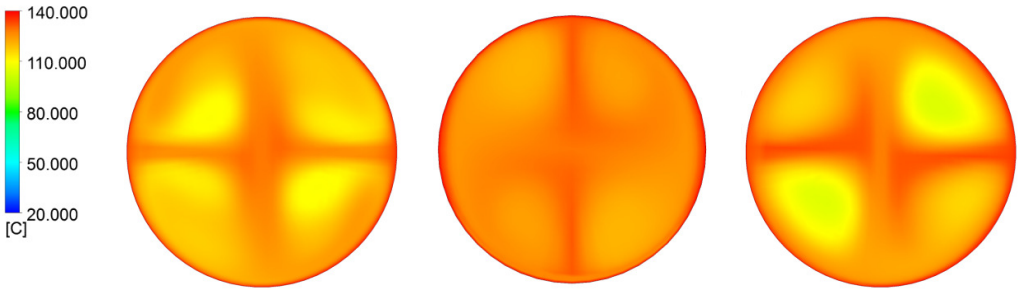

(a) (b) (c)

Figure 15: Effects of frequency of step rotation of vibration orientation on temperature distribution at pipe exit of vibrated viscous flow: (a) $\Omega = 0.2$ Hz; (b) $\Omega = 0.1$ Hz; (c) $\Omega = 0.067$ Hz. $T_{in} = 20$ °C; $T_w = 140$ °C; $D = 30$ mm; $L = 2400$ mm; = 4.0 cm s^{-1}; $\mu = k_0 \exp(E_a/R_g T)$ Pa s; $\rho = 998$ kg m^{-3}; $C_p = 4180$ J kg^{-1} K^{-1}; $\lambda = 0.668$ W m^{-1} K^{-1}; $A = 2$ mm; $f = 50$ Hz.

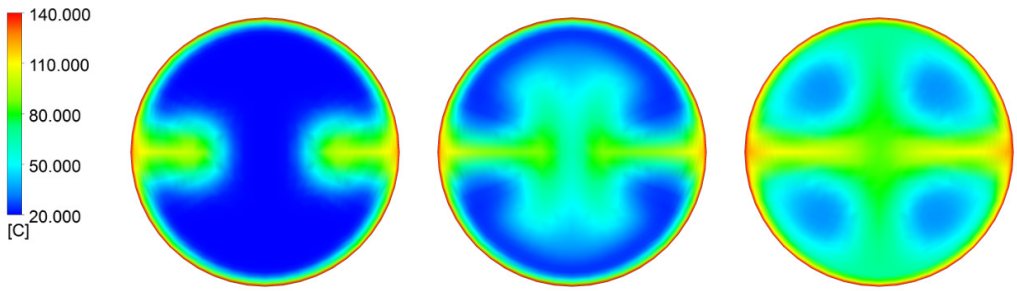

Figure 16: Effect of step rotation frequency on radial flow and temperature distribution: (a) $\Omega = 0.2$ Hz ($\Delta t = 5$ s; $z = 0.2$ m); (b) $\Omega = 0.1$ Hz ($\Delta t = 10$ s; $z = 0.4$ m); (c) $\Omega = 0.067$ Hz ($\Delta t = 15$ s; $z = 0.6$ m).
$T_{in} = 20$ °C; $T_w = 140$ °C; $D = 30$ mm; $L = 2400$ mm; = 4.0 cm s^{-1}; $\mu = k_0 \exp(E_a/R_g T)$ Pa s; $\rho = 998$ kg m^{-3}; $C_p = 4180$ J kg^{-1} K^{-1}; $\lambda = 0.668$ W m^{-1} K^{-1}; $A = 2$ mm; $f = 50$ Hz.

Highlights

- Transverse vibration with a step rotation of orientation has many benefits
- Wall heat transfer in viscous pipe flow is greatly enhanced
- Much improved radial temperature uniformity is achieved
- Thermal boundary layer grows rapidly along the pipe
- Short processing pipes can be used for heating of viscous fluid flow